Cancer Cell International

RESEARCH

Open Access

PHI-501, a dual inhibitor of RAF and DDR1/2, overcomes MAPK drug resistance in Melanoma

Sue Min Kim[1,2], Sungmin Cho[1,2], Gi-Jun Sung[3], Ky-Youb Nam[3], JeongHyeok Yoon[3], Taebo Sim[4,5,6,7], Joong Bae Ahn[2,8] and Sang Joon Shin[2,8*]

Abstract

Background Melanoma, an aggressive skin cancer caused by BRAF or NRAS mutations, is characterized by the hyperactivation of the MAPK pathway. Despite the initial clinical success of RAF and MEK inhibitors in BRAF V600E-mutant melanoma, resistance mechanisms, including MAPK pathway reactivation, compromise their efficacy. This study investigated PHI-501, a next-generation pan-RAF/DDR dual inhibitor, as a potential strategy for overcoming this resistance.

Methods The anti-proliferative activity of PHI-501 was evaluated in parental and acquired drug-resistant melanoma cell lines and compared with clinically relevant RAF inhibitors. Mechanistic studies included analyses of ERK, AKT, and DDR1/2 phosphorylation, as well as transcriptomic profiling of resistance-associated pathways. In vivo efficacy was assessed using xenograft models of SK-MEL-3 melanoma cells with acquired resistance to dabrafenib alone or to combined dabrafenib plus trametinib treatment.

Results PHI-501 exhibited greater cytotoxic activity than conventional RAF inhibitors in acquired drug-resistant melanoma cells. PHI-501 suppressed MAPK and PI3K/AKT signaling, as evidenced by reduced phosphorylation of ERK, AKT, and DDR1/2. Transcriptomic profiling revealed coordinated downregulation of key resistance-associated signaling pathways. In xenograft models derived from melanoma cells resistant to RAF inhibitor monotherapy or combined RAF/MEK inhibition, PHI-501 significantly inhibited tumor growth.

Conclusion PHI-501 exhibited potent anti-tumor activity in models of drug-resistant melanoma through dual targeting of RAF and DDR1/2. These findings support further preclinical evaluation of PHI-501 for MAPK inhibitor–resistant melanoma.

Keywords PHI-501, pan-RAF inhibitor, Discoidin domain receptor, MAPK pathway, drug resistance, melanoma, targeted therapy, BRAF, cancer, drug development

*Correspondence:
Sang Joon Shin
SSJ338@yuhs.ac

Full list of author information is available at the end of the article

Background

Melanoma, an aggressive form of skin cancer with high metastatic potential, presents notable challenges in advanced stages owing to its poor prognosis [1, 2]. Genetic alterations, particularly mutations in BRAF and NRAS, are frequently observed in melanomas. These mutations result in hyperactivation of the mitogen-activated protein kinase (MAPK) pathway, which drives uncontrolled cell proliferation and tumor progression [3]. Targeted therapies such as BRAF and MEK inhibitors have demonstrated significant clinical success in patients with BRAF (V600E) mutations [4]. However, their long-term effectiveness is frequently compromised by both intrinsic and acquired resistance, representing a major unresolved challenge in melanoma treatment.

Current first-line therapies for advanced or metastatic melanoma are primarily determined by BRAF mutational status. For BRAF V600-mutant melanoma, which accounts for approximately 45% of cases, the standard of care (SoC) consists of combined BRAF and MEK inhibition [5, 6]. FDA-approved regimens based on type I BRAF inhibitor–MEK inhibitor combinations, such as dabrafenib plus trametinib, encorafenib plus binimetinib, and vemurafenib plus cobimetinib, have significantly improved clinical outcomes, achieving objective response rates (ORR) of 64–76% and extending median progression-free survival (PFS) to 11–14.5 months, compared to only 5–8 months with BRAF inhibitor monotherapy [7, 8]. Despite these initial gains, the durability of response is limited by the inevitable emergence of acquired resistance, typically within 9–11 months [9].

Reactivation of MAPK signaling, including RAF dimer–dependent paradoxical activation associated with type I RAF inhibitors, represents a key limitation of current therapeutic strategies. Type II RAF inhibitors are currently being developed to mitigate this paradoxical activation. These inhibitors target both active and dimeric RAF complexes, offering broader efficacy against BRAF V600E, NRAS-mutant melanoma, and BRAF non-V600E (Class II/III) mutations [10, 11]. Several Type II RAF inhibitors are currently undergoing clinical trials, including tovorafenib (DAY101), naporafenib (Erasca, Phase 3), belvarafenib (Hanmi, Phase 1b), exarafenib (Kinnate, Phase 1b), and NST-628 (Nested Therapeutics, Phase 1) [12–14]. Notably, tovorafenib (DAY101) has recently become the first type II RAF inhibitor to receive FDA approval as a monotherapy for pediatric patients with relapsed or refractory low-grade glioma (LGG) harboring BRAF fusions, rearrangements, or V600 mutations, highlighting the clinical potential of this class of drugs beyond melanoma [15–16].

Discoidin domain receptors DDR1 and DDR2 are collagen-activated receptor tyrosine kinases that regulate tumor–extracellular matrix (ECM) interactions and promote invasion, migration, and survival in melanoma and other cancers [17, 18]. In melanoma, DDR1/2 expression increases with disease progression and contributes to matrix-mediated tolerance to MAPK-targeted therapies, in part through NF-κB–associated survival signaling [19]. Preclinical studies have shown that DDR inhibition can exert direct anti-tumor effects as monotherapy in collagen-rich contexts and can further enhance the efficacy of BRAF/MEK inhibitors by overcoming ECM-driven adaptive resistance in melanoma models [20, 21]. Early clinical evidence supporting DDR targeting has emerged from multi-kinase inhibitors with anti-DDR activity, such as dasatinib and sitravatinib, although selective DDR1/2 inhibitors remain in early stages of clinical development [22, 23].

PHI-501 is a novel, orally bioavailable Type II pan-RAF/DDR dual inhibitor specifically designed to suppress both RAF signaling and DDR1/2 activity. By concurrently targeting these pathways, PHI-501 aims to provide a broader spectrum of pathway inhibition, addressing key resistance mechanisms such as paradoxical MAPK reactivation and ECM-mediated survival signaling. Reflecting its clinical potential, PHI-501 recently achieved a significant regulatory milestone, receiving Investigational New Drug (IND) approval from the Ministry of Food and Drug Safety (MFDS) of the Republic of Korea in 2025, enabling initiation of a Phase 1 clinical trial.

In this study, we evaluated the therapeutic potential of PHI-501 in both parental and drug-resistant melanoma models. PHI-501 demonstrated superior antiproliferative effects compared to conventional RAF and MEK inhibitors in multiple melanoma cell lines. Mechanistically, PHI-501 effectively suppressed the MAPK and PI3K/AKT/mTOR pathways, induced transcriptional reprogramming, and significantly reduced tumor growth in xenograft models derived from resistant melanoma cells. These findings suggest that PHI-501 is a promising therapeutic candidate to address the unmet clinical need to overcome resistance to melanoma therapy.

Methods

Cell culture

SK-MEL-2, SK-MEL-3, A375P, and A375M cells were purchased from the Korean cell line bank. SK-MEL-24, SK-MEL-28, SK-MEL-29, RPMI7951, and SH4 cells

were purchased from the American Type Culture Collection (ATCC) and SK-MEL-30 cells were purchased from Deutsche Sammlung von mikroorganismen und Zellkulturen (DSMZ). Cells were maintained in Dulbecco's Modified Eagle's Medium (DMEM) or Roswell Park Memorial Institute 1640 medium (RPMI 1640) supplemented with 10% fetal bovine serum (FBS) and 1% penicillin-streptomycin at 37 °C and 5% CO_2.

Generation of drug-resistant cell lines

To generate drug-resistant melanoma cell lines, parental cells were seeded in 100-mm tissue culture dishes and, after 24 h, exposed to the indicated drug(s) at an initial concentration corresponding to 1/100 of the parental GI_{50}. Cells were continuously maintained under drug pressure with subculturing performed every 72 h, followed by re-exposure to drug(s) on the subsequent day. Drug concentrations were increased in a stepwise manner (1.5–2-fold) once cells regained stable proliferative capacity comparable to that of parental cells. This escalation process was continued over prolonged culture until cells exhibited sustained growth at the target selection dose. To comprehensively validate the establishment and stability of acquired resistance, each drug-resistant melanoma model was characterized using multiple complementary approaches. These included (i) CCK-8–based cytotoxicity assays to quantify drug sensitivity, (ii) clonogenic survival assays to assess long-term proliferative capacity under drug treatment, (iii) immunoblot analysis of MAPK and related signaling pathways, (iv) transcriptomic profiling by RNA sequencing, and (v) in vivo xenograft studies to evaluate resistance phenotypes in a physiological context. Collectively, these analyses confirmed the successful establishment and stability of chronic acquired-resistant melanoma models.

PHI-501 compound sourcing and preparation

PHI-501 was provided by Pharos iBio Co., Ltd. The compound was of GMP grade (Batch No. 30012A001) with a purity of 98.31% (as-is basis), as confirmed by the certificate of analysis. Identity was verified by FT-IR spectroscopy, and the levels of related substances, residual solvents, water content, and elemental impurities were all within acceptable specification limits. PHI-501 was dissolved in 100% DMSO to prepare a stock solution and stored at − 20 °C until use.

In vivo xenograft study

SK-MEL-3DR cells were subcutaneously injected into the right flank of 6-week-old BALB/c nude mice. Mice were randomly assigned to each group ($n = 9$ per group). Treatment was initiated when the tumor volume reached approximately 200 mm^3. The vehicle or respective drug was administered orally once daily for dabrafenib and twice daily for PHI-501 for 16 consecutive days. Tumor volume and body weight were measured daily. The tumor volume (mm^3) was calculated as $(L \times W^2)/2$. Tumor growth inhibition (TGI) was calculated as follows: TGI = [(tumor volume of control group) − (tumor volume of treated group)] / (tumor volume of control group) × 100.

Cell preparation for SDS-PAGE

Cells were washed twice with PBS and harvested using radioimmunoprecipitation assay (RIPA) buffer (ELPIS Biotech, Daejeon, South Korea) containing a protease inhibitor cocktail (GenDEPOT, Barker, TX, USA). The samples were centrifuged at 13,000 rpm for 10 min at 4 °C, and the supernatants were collected in fresh e-tubes for RIPA of soluble samples. Protein concentration was measured using the Bradford protein assay (BIO RAD, Hercules, CA, USA) and 5× SDS sample buffer (Biosesang, Yongin, South Korea) was added to the samples and heated at 95 °C for 5 min.

Western blotting

Equal amounts of protein in SDS sample buffer were resolved on 12% polyacrylamide Bis-Tris gels in running buffer (25 mM Tris, 250 mM glycine, 0.1% SDS) using sodium dodecyl sulfate-polyacrylamide gel electrophoresis (SDS-PAGE). Proteins were then transferred to a polyvinylidene fluoride (PVDF) membrane (Merck Millipore, Darmstadt, Germany) and blocked with 5% BSA in TBST (0.1% Tween-20 in TBS) for 1 h at room temperature. The membranes were incubated overnight at 4 °C with primary antibodies diluted in 5% BSA in TBST as indicated in the text: p-DDR1 (Cell Signaling Technology, CST14531), p-DDR1/2 (R&D Systems, MAB25382), p-AKT (Cell Signaling Technology, CST4058), AKT (Cell Signaling Technology, CST9272), p-MEK (Cell Signaling Technology, CST9121), p-ERK (Cell Signaling Technology, CST9101), ERK (Cell Signaling Technology, CST9102), Cyclin D1(Cell Signaling Technology, CST2978), and Survivin (Cell Signaling Technology, CST2808). After washing, the membranes were incubated with goat anti-rabbit or goat anti-mouse secondary antibodies conjugated to horseradish peroxidase (Invitrogen, Carlsbad, CA, USA). diluted in 1× TBS for 1 h, and immunoreactivity was detected using an enhanced chemiluminescence substrate for horseradish peroxidase (HRP) (Elpisbio, Daejeon,

Korea; #EBP-1071), followed by chemiluminescence imaging (ImageQuant 800). Each membrane was re-validated with anti-GAPDH (Santa Cruz Biotechnology, sc-32233) or β-actin (Santa Cruz Biotechnology, sc-47778) antibodies and used as a control for protein quantification.

Cell viability assay

To quantify cell viability under each experimental condition, the CCK-8 assay was performed using the Cell Counting Kit-8 assay (Dojindo, Kumamoto, Japan) following the manufacturer's instructions. Cells were seeded in a 96-well cell culture plate and treated with various concentrations of the drug for 48 h. Ten microliters of CCK-8 solution was added to each well of the plate and incubated for 2–4 h in an incubator. The absorbance was measured at 450 nm using a microplate reader (VERSA Max).

Clonogenic assay

Cells were seeded at a low density of 100–200 cells per well in six-well culture plates, depending on the growth characteristics of each cell line, and allowed to adhere overnight. Following seeding, plates were not moved to minimize satellite colony formation. The next day, the indicated compounds were added to the culture medium without changing the medium, and drug treatment was maintained throughout the 14-day incubation period. After 14 days, colonies were gently washed with PBS, fixed, and stained for 30 min at room temperature using a solution containing 0.5% (w/v) crystal violet (Sigma, V5265), 20% methanol, and 4% paraformaldehyde in PBS. Colonies consisting of ≥ 50 cells per colony were counted manually.

Bioinformatical analysis of RNA-seq data

RNA sequencing (RNA-seq) was performed on five melanoma cell lines, including both parental and resistant models, with three biological replicates per condition. Total RNA was extracted and sequenced by Macrogen Inc., using the Illumina HiSeq 2500 platform. Raw sequencing data were processed for quality control, read alignment, and quantification of the transcripts. Differential expression analysis was conducted using DESeq2 in R. GSEA was performed using GSEA software version 4.2.3, with hallmark gene sets (h.all.v7.0. symbols.gmt), and KEGG (c2.cp.kegg.v6.1. symbols.gmt) to assess pathway-level changes following PHI-501 treatment. The enrichment results were ranked based on normalized enrichment scores (NES) and false discovery rates (FDR < 0.25). Visualizations, including Principal component analysis (PCA) plots, heat maps, and bubble plots, were generated using R (v4.4.3) and GraphPad Prism (v7.0).

Whole-exome sequencing and variant analysis

Whole-exome sequencing (WES) was performed on parental melanoma cell lines (A375 and SK-MEL-2) and their independently derived acquired-resistant counterparts (A375DTR and SK-MEL-2BR). Genomic DNA was extracted using standard protocols, and exome sequencing was conducted by Macrogen Inc. Exome libraries were prepared using the SureSelect V6-Post capture kit and sequenced using a high-throughput run mode with a paired-end read length of 101 bp × 2.

Single-nucleotide variants (SNVs) were identified from WES data and annotated using ClinVar clinical significance (CLINSIG_CLINVAR) and gnomAD allele frequency (gnomAD_AF) databases. Variants were filtered to retain those classified as *Likely pathogenic*, *Likely risk allele*, *Pathogenic*, *Pathogenic/Likely pathogenic*, or *risk factor*, with an additional filtering criterion of gnomAD_AF < 0.001. To facilitate focused analysis, a predefined variants-of-interest gene set comprising 41 genes was curated, encompassing MAPK pathway core components, RTK/PI3K bypass signaling, melanoma lineage regulators, and adaptive/DDR-related pathways.

Copy number variation (CNV) analysis was performed using WES BAM files by calculating read depth ratios across genomic regions. Chromosomal coordinates were annotated to corresponding genes based on the human reference genome (hg38). CNV states were defined according to read depth ratio thresholds as follows: deletion (< 0.25×), loss (< 0.5×), gain (> 2×), and amplification (> 4×). Genome-wide CNV profiles, chromosome-level CNV distributions, and gene-level copy number alterations were compared between parental and acquired-resistant melanoma cell lines.

Quantification and statistical analysis

All statistical analyses were performed using R software (version 4.4.3) and GraphPad Prism (v7.0). Data are presented as the mean ± SEM of at least three independent experiments.

Survival analysis: Kaplan–Meier survival curves were generated using the GEPIA2 web tool (http://gepia2.cancer-pku.cn) for overall survival and disease-free survival across all TCGA solid cancer types. Patients were

stratified into high (top 25%) and low (bottom 25%) expression groups for both DDR1 and DDR2 expression. Statistical significance was determined using the log-rank test for survival analysis.

Proteomic analysis: Reverse phase protein array (RPPA) data for skin cutaneous melanoma (SKCM) samples were obtained from The Cancer Genome Atlas (TCGA) and Cancer Cell Line Encyclopedia (CCLE). Differentially expressed proteins were identified using the limma2 package (3.62.2) in R, and a volcano plot was constructed to visualize significant changes, with log2 fold-change on the x-axis and −log10(p-value) on the y-axis.

Correlation analysis: Heat maps displaying correlation patterns were generated using the pheatmap package in R Studio, and Pearson correlation coefficients were calculated between DDR1/2 and key signaling proteins. Statistical significance is denoted by * $p < 0.05$, ** $p < 0.01$, and *** $p < 0.001$. The relationship between gene expression and inhibitor sensitivity was evaluated using expression data from the DepMap portal (24Q4 release) (https://depmap.org/portal/) and drug response data from the Genomics of Drug Sensitivity in Cancer (GDSC2) database (https://www.cancerrxgene.org).

Comparisons between experimental groups: Statistical comparisons between two groups were conducted using an unpaired two-tailed Student's t-test, while comparisons involving multiple groups were analyzed using one-way analysis of variance (ANOVA) followed by Tukey's post hoc test.

Multiple comparison correction: P-values less than 0.05 were considered statistically significant. For multiple comparisons, p-values were adjusted using the Benjamini–Hochberg method to control the false discovery rate.

Reporting statistical details: Statistical significance was defined as $^{*}p < 0.05$, $^{**}p < 0.01$, and $^{***}p < 0.001$, unless otherwise indicated. Specific statistical tests, significance levels, and number of biological replicates are provided in the figure legends.

Reagents and resources

All antibodies, reagents, chemical compounds, cell lines, animal models, datasets, and software used in this study are listed in Supplementary Table S3, along with vendor information, catalog numbers, and Research Resource Identifiers (RRIDs).

Results

MAPK inhibitor-resistant melanoma cells exhibit enhanced DDR1/2 related signaling

To elucidate the mechanisms underlying resistance to MAPK pathway inhibitors, we established drug-resistant melanoma cell lines by chronically exposing SK-MEL-2, SK-MEL-3, and A375 cells to RAF and MEK inhibitors. BRAF V600E–mutant SK-MEL-3 and A375 cells were selected for resistance to dabrafenib and trametinib, reflecting the standard targeted therapies used in BRAF-mutant melanoma. In contrast, NRAS-mutant SK-MEL-2 cells (Q61R), which are generally less responsive to type I RAF inhibitors due to MAPK pathway reactivation, were exposed to the type II RAF inhibitor belvarafenib, which has shown activity in NRAS-mutant melanoma models. Using this approach, we generated belvarafenib-resistant SK-MEL-2 (SK-MEL-2BR) and dabrafenib-, trametinib-, or dual-resistant derivatives of SK-MEL-3 and A375 cells (SK-MEL-3DR/TR/DTR and A375DR/TR/DTR). These cell lines exhibited robust resistance phenotypes, as validated by clonogenic assays. While parental cell lines exhibited near-complete inhibition of colony formation at 0.1–0.3 μM, drug-resistant cell lines displayed minimal inhibition across this range, with sustained or enhanced clonogenic survival observed at higher concentrations (Fig. 1a, b). Resistant cell lines demonstrated substantial increases in half-maximal growth inhibitory concentration (GI_{50}) values, ranging from tens-fold to several thousand-fold increases, with GI_{50} values for dabrafenib and belvarafenib being indeterminable, confirming a profound loss of drug sensitivity (Fig. 1c; Table S1). Consistent with these functional resistance phenotypes, basal pERK levels were maintained or increased in resistant models relative to parental cells. Whereas parental cells showed clear pERK suppression upon exposure to the corresponding MAPK pathway inhibitor(s) used to generate resistance, resistant cells failed to suppress pERK under the same treatments (Fig. 1d).

RNA sequencing and Gene Set Enrichment Analysis (GSEA) of parental and drug-resistant melanoma cells revealed altered MAPK pathway activity indicators, consistent with the increased p-ERK levels observed in western blot analysis (Fig. 1e). Notably, KRAS signaling DN was consistently downregulated across all four drug-resistant cell lines, whereas KRAS signaling UP and mTORC1 signaling were enriched in belvarafenib- and trametinib-resistant cells (Fig. 1e). GSEA also revealed the upregulation of several other pathways, including the P53 pathway, apoptosis, IL-2/STAT5

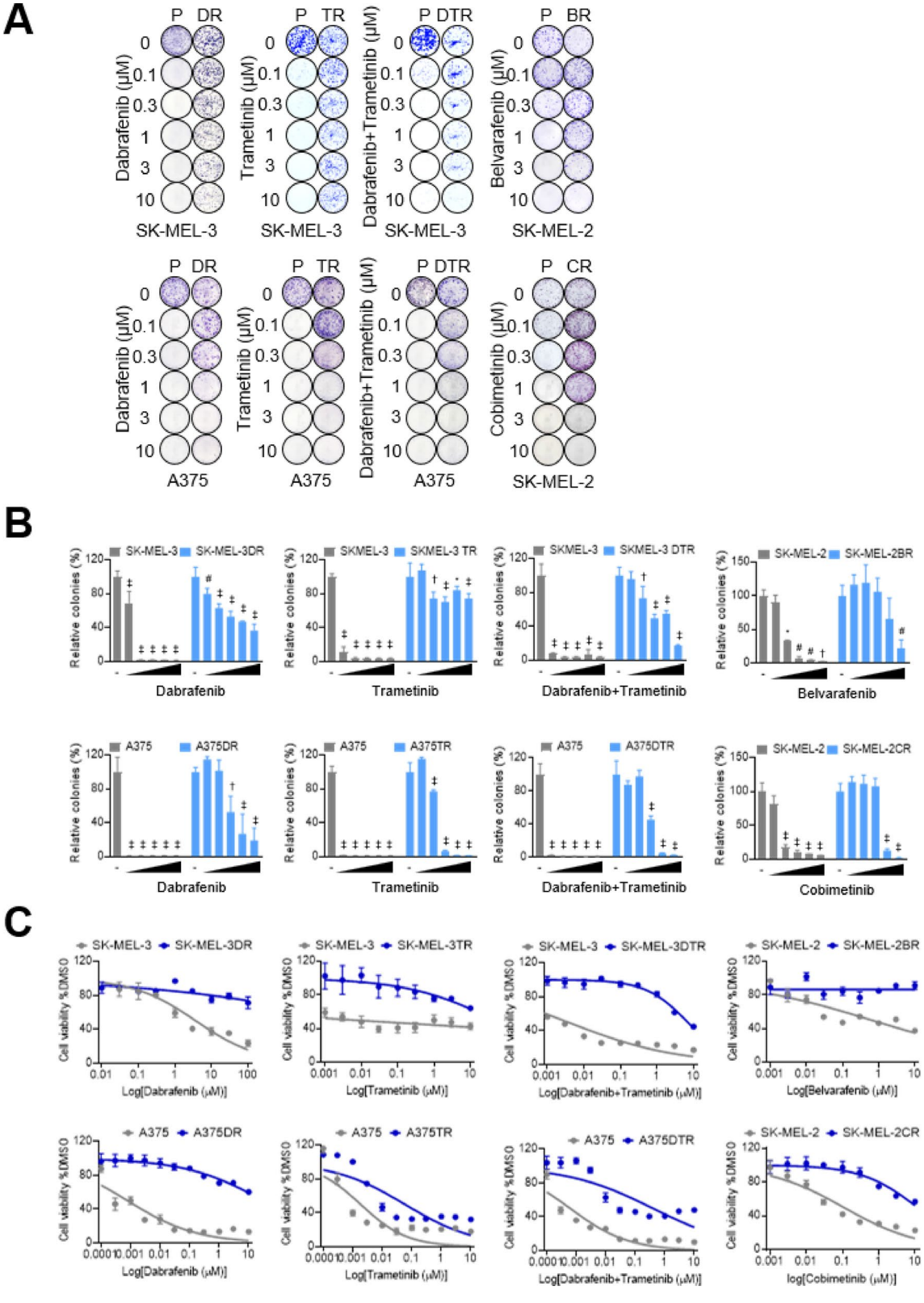

Fig. 1 (See legend on next page.)

(See figure on previous page.)

Fig. 1 MAPK inhibitor-resistant melanoma cells exhibit enhanced DDR1/2 signaling. (**A**) Clonogenic assay showing the validation of drug-resistant cell lines. (**B**) Quantification of clonogenic assay shown in Fig. 1A. Data are presented as relative colony formation (%) normalized to the control group and expressed as the mean ± SEM, $n = 3$ replicates. Statistical significance was determined by two-way ANOVA. * $p < 0.05$, # $p < 0.001$, † $p < 0.001$, ‡ $p < 0.0001$. (**C**) Cell viability assay of RAF and MEK inhibitors in parental cells and drug-resistant cells for 48 h. Data are presented as the mean ± SEM, $n = 3$ replicates. (**D**) Western blot analysis of pERK and pAKT signaling responses in parental and resistant melanoma cells following 48-h treatment with vehicle or the corresponding resistance-selecting drug(s) at 1 μM. (**E**) Bubble plot representing Gene Set Enrichment Analysis (GSEA) using hallmark gene set comparing parental and resistant melanoma cells. Pathway enrichment was calculated using GSEA, with color indicating NES (blue = downregulated, red = upregulated) and bubble size representing −log10(p-value). (**F**) SK-MEL-2 and SK-MEL-2BR cells were stimulated with type I collagen (40 μg/ml) for 18 h to activate DDR signaling

signaling, and IL-6/JAK/STAT3 signaling, in all resistant cell lines.

Moreover, epithelial-mesenchymal transition (EMT) was significantly upregulated in SK-MEL-2BR and SK-MEL-3TR cells (Fig. 1e). One of the key regulators of EMT in solid tumors is discoidin domain receptors (DDRs), a family of collagen-binding receptor tyrosine kinases (RTKs) that integrate extracellular matrix (ECM)-derived signals to modulate cell adhesion, migration, and survival [24, 25]. DDRs play a critical role in ECM remodeling, tumor invasion, and pro-survival signaling, contributing to therapeutic resistance in various cancers, including melanoma [26]. Additionally, IL-6/JAK/STAT3 and TNF-α/NF-κB signaling pathways, both of which are modulated by DDR activity, were among the most enriched pathways in drug-resistant melanoma cells, further linking DDR activation to adaptive stress responses associated with acquired resistance [27, 28]. Whole-exome sequencing analysis showed no substantial changes in major driver mutations or genome-wide alteration patterns in A375DTR and SK-MEL-2BR compared with their respective parental melanoma cells (Supplementary Fig. S1a-S1j).

To explore whether DDR activation in drug-resistant melanoma cells is functionally linked to their ability to survive MAPK inhibition, we examined the effects of collagen stimulation on DDR signaling. Collagen stimulation significantly enhanced DDR1 phosphorylation in SK-MEL-BR cells but not in parental cells, suggesting that DDR signaling is not only upregulated in resistant melanoma but is also more responsive to ECM-derived signals (Fig. 1f).

DDR1 and DDR2 are associated with MAPK pathway activation and therapeutic resistance in melanoma

We analyzed pan-cancer survival data from The Cancer Genome Atlas (TCGA) to assess the clinical relevance of DDR1 and DDR2 expression in cancer progression. Kaplan–Meier analysis showed a significant association between high DDR2 expression and poorer overall survival (HR = 1.2, $p = 0.00032$). In contrast, although high DDR1 expression showed a trend toward poorer survival, this association did not reach statistical significance (HR = 1.1, $p = 0.076$) (Fig. 2a).

To identify activated signaling networks in BRAF- and NRAS-mutant melanoma, we performed proteomic profiling of SKCM samples using RPPA data obtained from TCGA and the Cancer Cell Line Encyclopedia (CCLE). This analysis revealed the upregulation of total AKT and phosphorylated MEK1, indicating the activation of the MAPK and PI3K/AKT pathways (Fig. 2b and Supplementary figure S2a).

Subsequently, we assessed the relationship between DDR1/2 expression and key MAPK and AKT pathway genes in TCGA–SKCM melanoma samples (Fig. 2c). Both DDR1 and DDR2 were significantly positively correlated with MAPK-related genes (RAF1, BRAF, MAPK1, and MAP2K1) and AKT pathway genes (AKT1, AKT2, AKT3, PIK3CA, PIK3CB, PTEN, and MTOR). In the CCLE–SKIN dataset, DDR1 expression was significantly correlated with AKT3 and PIK3CD, whereas DDR2 expression was correlated with MAP2K2, BRAF, KRAS, AKT3, and MTOR (Supplementary Figure S2b).

Based on these observations, we assessed whether DDR1 expression could predict the sensitivity of melanoma cell lines to MAPK pathway inhibitors. We correlated DDR1 levels (DepMap) with LN(IC_{50}) values from GDSC2 for dabrafenib and trametinib. DDR1 expression was positively associated with LN(IC_{50}) for both drugs (dabrafenib: $r = 0.416$, $p = 0.0221$, $N = 30$; trametinib: $r = 0.376$, $p = 0.0338$, $N = 32$), indicating that higher DDR1 levels corresponded to reduced sensitivity (Fig. 2d). DDR1 expression also showed significant positive correlations with LN(IC_{50}) values across a broader panel of 11 MAPK pathway inhibitors, supporting DDR1 as a predictive marker of MAPK inhibitor response (Supplementary Figure S2c).

These findings indicate that DDR signaling activation is functionally linked to MAPK and AKT signaling

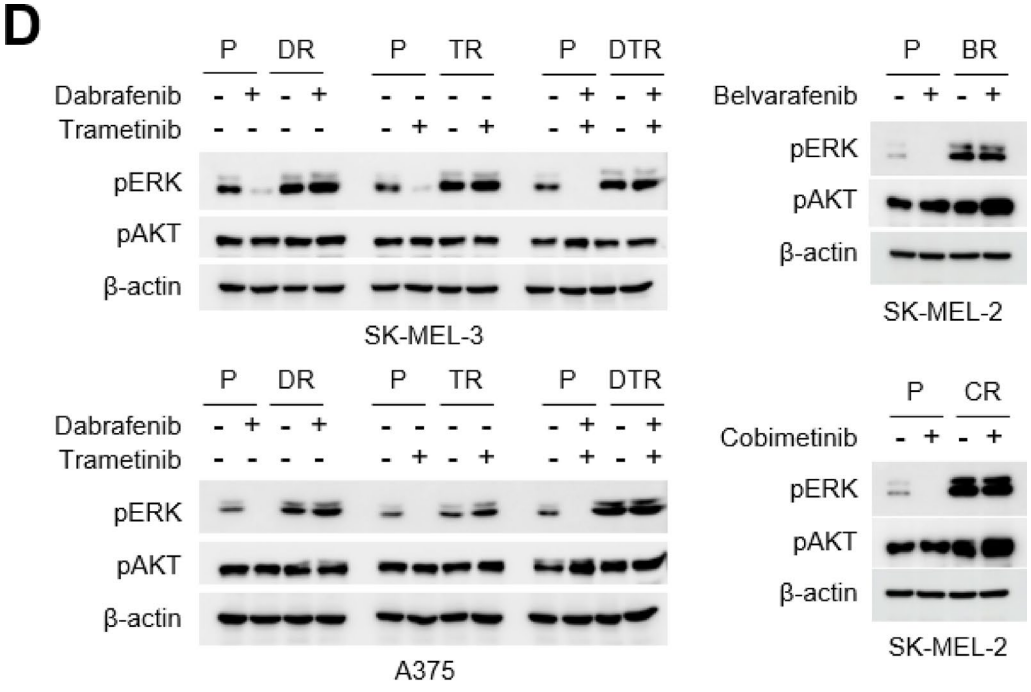

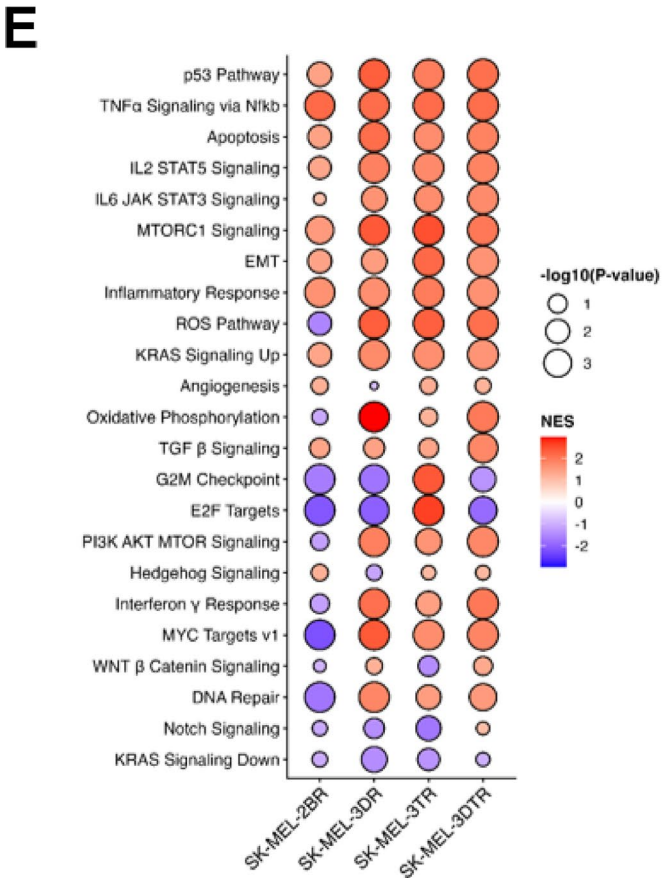

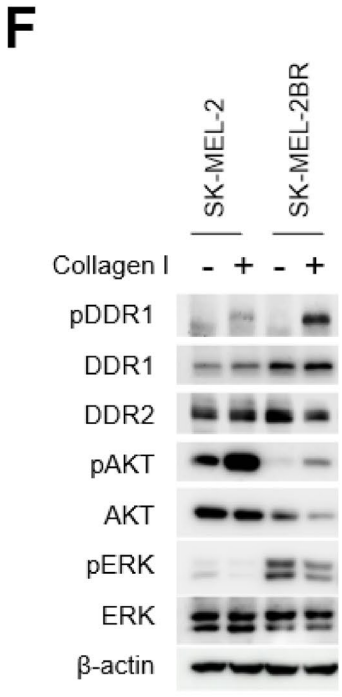

Fig. 1 (continued)

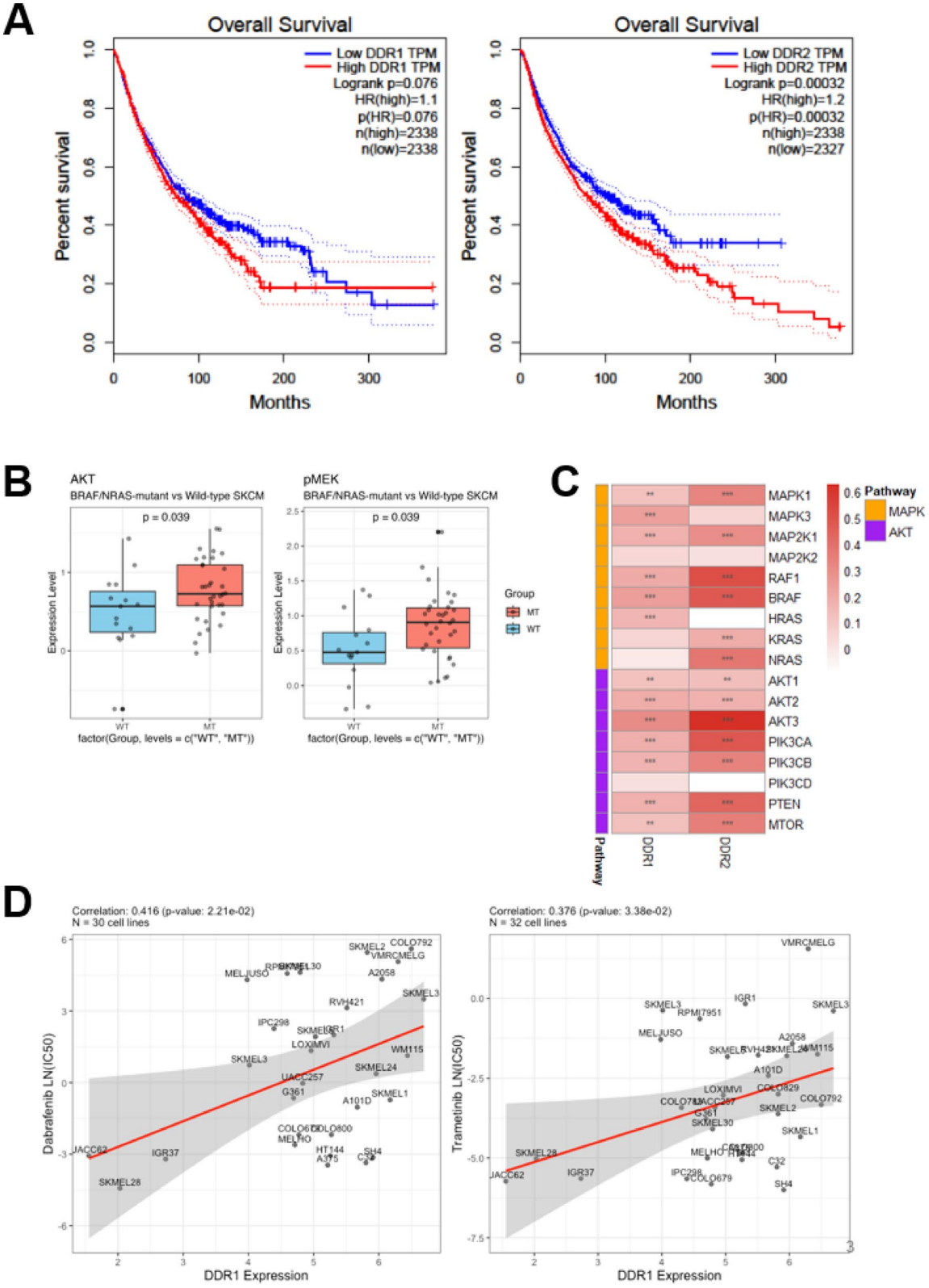

Fig. 2 (See legend on next page.)

(See figure on previous page.)

Fig. 2 DDR1 and DDR2 are associated with MAPK pathway activation and therapeutic resistance in melanoma. (**A**) Kaplan–Meier survival analysis showing patient outcomes based on DDR1 and DDR2 expression levels across all TCGA cancer types. Patients were stratified into high (top 25%) and low (bottom 25%) expression groups, and overall survival (OS) was analyzed. (**B**) Proteomic analysis of BRAF/NRAS-mutant SKCM. Box plots demonstrate differential expression of AKT and phosphorylated MEK1 (pMEK1-S217/S221) between wild-type and mutant groups. (**C**) Correlation heatmaps between DDR1/2 and key genes in the MAPK and AKT signaling pathways in TCGA-SKCM samples. Color intensity represents the correlation value, with red indicating a positive correlation. Significance levels are indicated by asterisks (* $p < 0.05$, ** $p < 0.01$, *** $p < 0.001$). (**D**) Correlation analysis revealing DDR1 expression (DepMap) and MAPK pathway inhibitor sensitivity (GDSC2) in melanoma cell lines. Scatter plots depicting correlations between DDR1 expression levels and IC50 to Dabrafenib (left) and Trametinib (right)

pathway activity in melanoma and support the co-targeting of RAF and DDR as a promising strategy to overcome MAPK inhibitor resistance in BRAF- and NRAS-mutant melanomas.

PHI-501 is a pan-RAF/DDR dual kinase inhibitor

PHI-501, a next-generation dual kinase inhibitor, targets both pan-RAF and DDRs. The chemical structure of PHI-501 is shown in Fig. 3a. To evaluate kinase selectivity, a comprehensive kinome-wide inhibition profiling assay was performed using 1 μM of PHI-501.

In silico docking models were generated to elucidate the molecular mechanisms of action. These models revealed that PHI-501 occupied the ATP-binding cleft of the representative kinase domains, forming predicted hydrogen bonds and hydrophobic interactions with conserved hinge-region residues (Fig. 3b).

The activity of PHI-501 against DDR kinases was evaluated using two orthogonal platforms: KINOMEScan screening across a 10-point dilution series revealed IC_{50} values of 0.30 nM for DDR1 and 8.57 nM for DDR2 (Fig. 3c). A HotSpot catalytic assay corroborated these findings, demonstrating inhibitory potencies of 15.12 nM for DDR1 and 2.15 nM for DDR2 (Fig. 3d).

To assess RAF family targeting, HotSpot dose-response assays were performed on recombinant ARAF, BRAF, BRAF V600E, CRAF, and additional BRAF V600 variants (V600A/D/E/K, G464V, and L597V). These assays yielded IC_{50} values ranging from 1.5 to 27.8 nM (Fig. 3e and f). An expanded HotSpot screen across diverse BRAF alterations, including non-V600 point mutants, insertion mutants, and oncogenic BRAF fusions, demonstrated IC_{50} values in the nanomolar range across all variant classes (Supplementary Figure S3a, S3b; Table S2).

We evaluated the anti-proliferative activity of PHI-501 in ten melanoma cell lines, including eight with BRAF V600E mutations and two with NRAS Q61 mutations. PHI-501 effectively suppressed the growth of all cell lines, with GI_{50} values ranging from 0.09262 to 2.058 μM. These results highlight the efficacy of PHI-501 against BRAF- and NRAS-induced melanomas (Fig. 3g). To further verify the selectivity of PHI-501, we evaluated its effects on three non-tumor fibroblast cell lines, including skin-derived (Detroit 551 and CCD-986sk) and colon-derived (CCD-18Co) fibroblasts. PHI-501 showed markedly higher GI_{50} values (28.16–91.67 μM) in these normal cells, confirming that its anti-tumor activity is not due to non-specific cytotoxicity (Fig. 3h).

PHI-501 inhibits MAPK signaling in both BRAF- and NRAS-mutant melanoma

PHI-501 inhibited DDR, MEK, ERK, and AKT phosphorylation in eight melanoma cell lines harboring BRAF V600E or NRAS Q61 mutants in a dose-dependent manner at 24 and 48 h post-treatment. Furthermore, it suppressed the expression of cyclin D1 and survivin, which are key markers of cell proliferation and differentiation (Fig. 4a and Supplementary Figure S4a).

To further investigate transcriptional changes induced by PHI-501, RNA-seq was performed in SK-MEL-2 and SK-MEL-3 cells, which revealed widespread alterations in gene expression (Supplementary Figure S34 and S4c). Subsequent GSEA analyses demonstrated significant downregulation of the MAPK signaling pathway and suppression of multiple oncogenic programs including E2F, MYC, and KRAS signaling (Fig. 4b and Supplementary Figure S4d and S4e).

To determine whether PHI-501 retained its inhibitory activity under collagen-induced DDR1 activation, SK-MEL-3 and A375 cells were treated with PHI-501 in the presence of collagen, and PHI-501 dose-dependently inhibited pDDR1, pERK, and pAKT levels (Fig. 4C and D, and Supplementary Figure S4F).

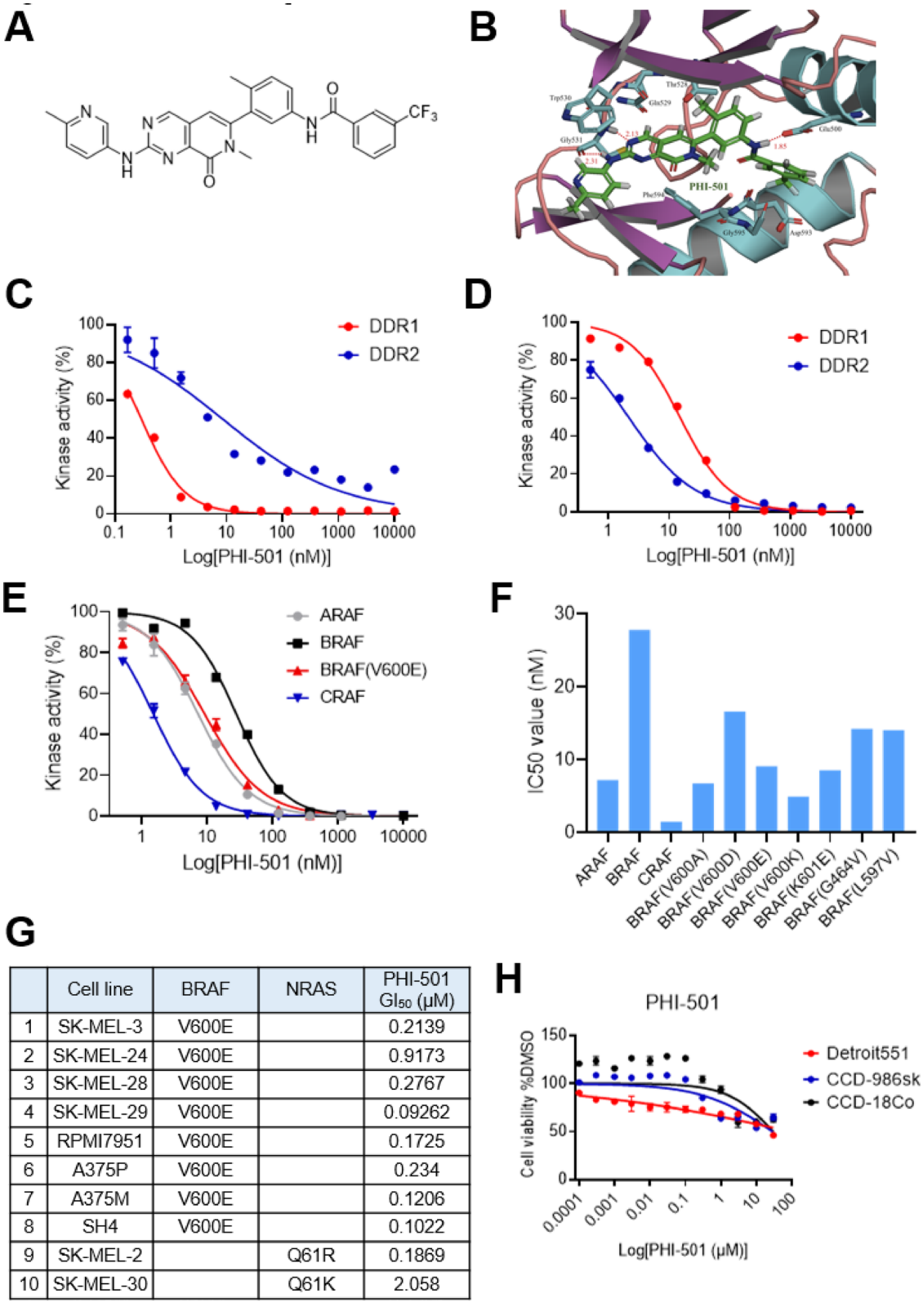

G

	Cell line	BRAF	NRAS	PHI-501 GI_{50} (μM)
1	SK-MEL-3	V600E		0.2139
2	SK-MEL-24	V600E		0.9173
3	SK-MEL-28	V600E		0.2767
4	SK-MEL-29	V600E		0.09262
5	RPMI7951	V600E		0.1725
6	A375P	V600E		0.234
7	A375M	V600E		0.1206
8	SH4	V600E		0.1022
9	SK-MEL-2		Q61R	0.1869
10	SK-MEL-30		Q61K	2.058

Fig. 3 (See legend on next page.)

(See figure on previous page.)

Fig. 3 PHI-501 is a novel pan-RAF/DDRs dual kinase inhibitor. (**A**) Chemical structure of PHI-501. (**B**) Predicted docking pose of PHI-501 within the ATP-binding pocket. (**C**) KINOMEScan profiling of PHI-501 against DDR1 and DDR2 across a concentration series. (**D**) Kinase HotSpot assay of PHI-501 inhibition of DDR1 and DDR2. (**E**) Kinase HotSpot assay of PHI-501 against ARAF, BRAF, BRAF V600E, and CRAF. (**F**) Kinase HotSpot Assay IC_{50} values (nM) for ARAF, BRAF, CRAF, and BRAF mutants (V600A, V600D, V600E, V600K, G464V, and L597V). (**G**) Half-maximal growth inhibitory concentration (GI_{50}) of PHI-501 in 10 melanoma cell lines harboring BRAF(V600E) or NRAS (Q61R or Q61K) mutations. PHI-501 (0.001–10 μM) or DMSO (vehicle) for 48 h. (**H**) Cell viability assay of PHI-501 in Detroit551, CCD-986sk, and CCD-18Co cells for 48 h

Type I RAF inhibitors such as vemurafenib and dabrafenib have been shown to induce paradoxical activation, particularly in RAS-mutant melanoma models, by promoting RAF dimerization and reactivating downstream signaling pathways. Consistent with this observation, in NRAS Q61K-mutant SK-MEL-2 cells, vemurafenib and dabrafenib failed to suppress ERK phosphorylation, with vemurafenib inducing paradoxical ERK activation as early as 2 h after treatment. Conversely, PHI-501 effectively inhibited ERK phosphorylation in a dose-dependent manner from 2 to 48 h, demonstrating sustained suppression of RAF-mediated signaling (Fig. 4e and f). In dose-response experiments, PHI-501 inhibited AKT phosphorylation starting at 0.1 μM, with complete inhibition observed at 1 and 10 μM. Conversely, vemurafenib activated ERK phosphorylation at all concentrations, whereas dabrafenib exhibited paradoxical activation at lower doses, with inhibition observed only at 10 μM (Fig. 4g and h). These findings suggest that PHI-501 overcomes paradoxical activation and provides broader suppression of adaptive survival signaling compared to Type I RAF inhibitors in both BRAF- and NRAS-mutant melanoma.

PHI-501 overcomes resistance to RAF and MEK inhibitors in melanoma cells

PHI-501 demonstrated enhanced inhibition of colony formation in a dose-dependent manner across resistant melanoma cell lines compared with belvarafenib, dabrafenib, trametinib, and the combination of dabrafenib plus trametinib. At concentrations as low as 0.1 μM, PHI-501 markedly reduced colony formation in all resistant cell lines examined. In contrast, resistant cells continued to form colonies following prolonged exposure to 10 μM belvarafenib, dabrafenib, trametinib, or dabrafenib plus trametinib (Fig. 5a, Supplementary figure S5A).

Cytotoxicity assays demonstrated that PHI-501 retains robust anti-proliferative activity across an expanded panel of acquired-resistant melanoma cell lines (Fig. 5b and c). Notably, PHI-501 maintained submicromolar GI_{50} values in BRAF-mutant resistant models, whereas dabrafenib and belvarafenib exhibited markedly reduced efficacy. In NRAS-mutant SK-MEL-2–derived resistant cells, PHI-501 remained active while dabrafenib lacked detectable cytotoxicity and belvarafenib displayed limited activity. In dual-resistant models, the standard-of-care dabrafenib plus trametinib combination showed higher GI_{50} values than PHI-501 monotherapy, with SK-MEL-3DTR at 16.61 μM versus 0.497 μM (≈ 33.4-fold) and A375DTR at 0.847 μM versus 0.262 μM (≈ 3.23-fold).

To benchmark PHI-501 against other inhibitors of the same pharmacological class, we further compared its anti-proliferative activity with additional type II RAF inhibitors, including naporafenib and tovorafenib, alongside belvarafenib, across a panel of eight melanoma cell lines comprising parental and acquired-resistant A375 and SK-MEL-3 models (Supplementary Figure S5B and S5C). Across both parental and resistant contexts, PHI-501 consistently exhibited the lowest GI_{50} values among the tested type II RAF inhibitors, indicating superior and more uniform potency. These results demonstrate that the enhanced anti-proliferative activity of PHI-501 is maintained even in direct comparisons within the type II RAF inhibitor class.

Across resistant melanoma models, MAPK pathway inhibitors did not consistently suppress MAPK signaling and were frequently accompanied by increased pAKT (Fig. 5D). Specifically, dabrafenib either failed to suppress pERK or required a high concentration (10 μM) to achieve inhibition, which was often accompanied by an increase in pAKT. While belvarafenib reduced pERK levels in certain cell lines, it was associated with the most pronounced induction of pAKT. In the dual-resistant SK-MEL-3DTR model, the standard-of-care dabrafenib plus trametinib combination failed to reduce pERK and increased pAKT. In contrast, PHI-501 suppressed pDDR1/2, pERK, and pAKT in both single- and dual-resistant models in a dose-dependent

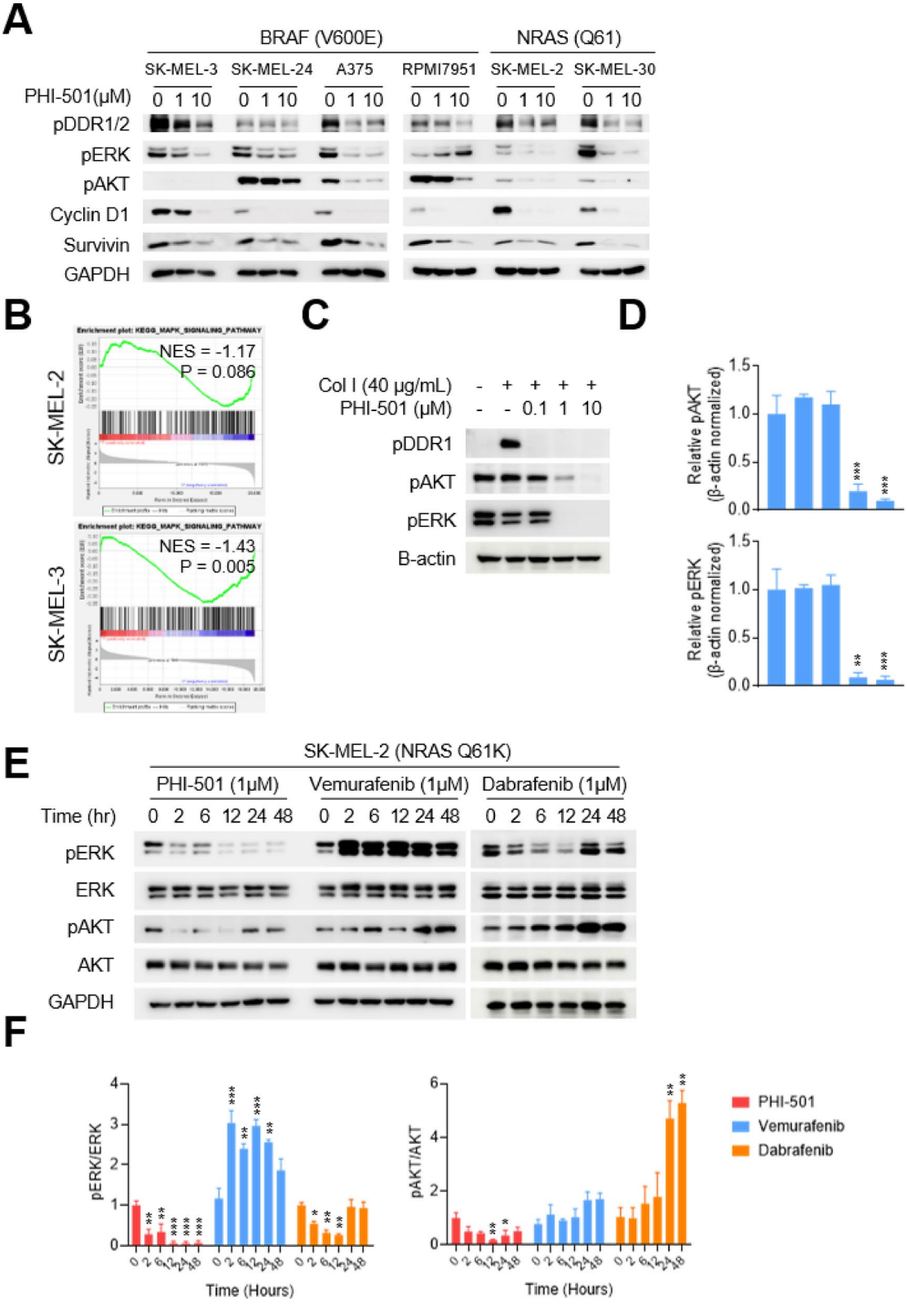

Fig. 4 (See legend on next page.)

(See figure on previous page.)

Fig. 4 PHI-501 inhibits MAPK signaling in both BRAF- and NRAS-mutant melanoma. (**A**) Western blot analysis of four BRAF-mutant and two NRAS-mutant melanoma cell lines treated with PHI-501 (1 and 10 μM) for 24 h. (**B**) SK-MEL-2 and SK-MEL-3 cells were treated with PHI-501 (10 μM) for 48 h, and GSEA was performed using the KEGG MAPK signaling pathway gene set. (**C**) Western blot analysis of the dose-dependent effect of PHI-501 on SK-MEL-3 cells under type I collagen (40 μg/ml) stimulation for 48 h. (**D**) Quantification of pAKT and pERK levels normalized to β-actin from the western blot analysis shown in (**C**). Data are presented as mean ± SEM from three independent experiments. (**E**) Time-dependent inhibitory effects of PHI-501 (1 μM) compared to vemurafenib (1 μM) in SK-MEL-2 cells. (**F**) Quantification of pERK normalized to total ERK and pAKT normalized to total AKT from the western blot analysis shown in (E). Data are presented as mean ± SEM from three independent experiments. (**G**) Dose-dependent inhibitory effects of PHI-501 compared to vemurafenib in SK-MEL-2 cells. (**H**) Quantification of pERK normalized to total ERK and pAKT normalized to total AKT from the western blot analysis shown in (G). Data are presented as mean ± SEM from three independent experiments

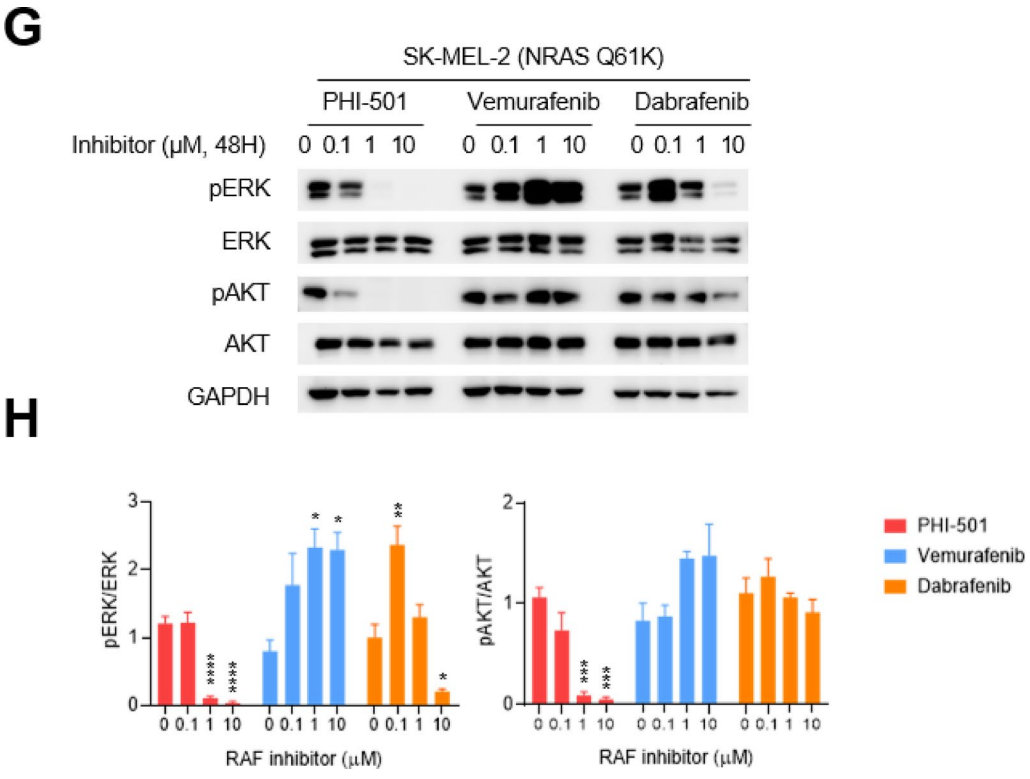

Fig. 4 (continued)

manner, with inhibition starting at 1 μM and substantial suppression at 10 μM. These observations suggest that PHI-501 effectively suppresses MAPK signaling while preventing the compensatory AKT activation commonly observed with conventional RAF and MEK inhibitors.

PHI-501 modulates transcriptional profiles in parental and resistant melanoma cells

To further elucidate transcriptional responses to PHI-501, we performed RNA sequencing on six melanoma cell lines, including parental and resistant cells. Principal component analysis (PCA) was performed for the

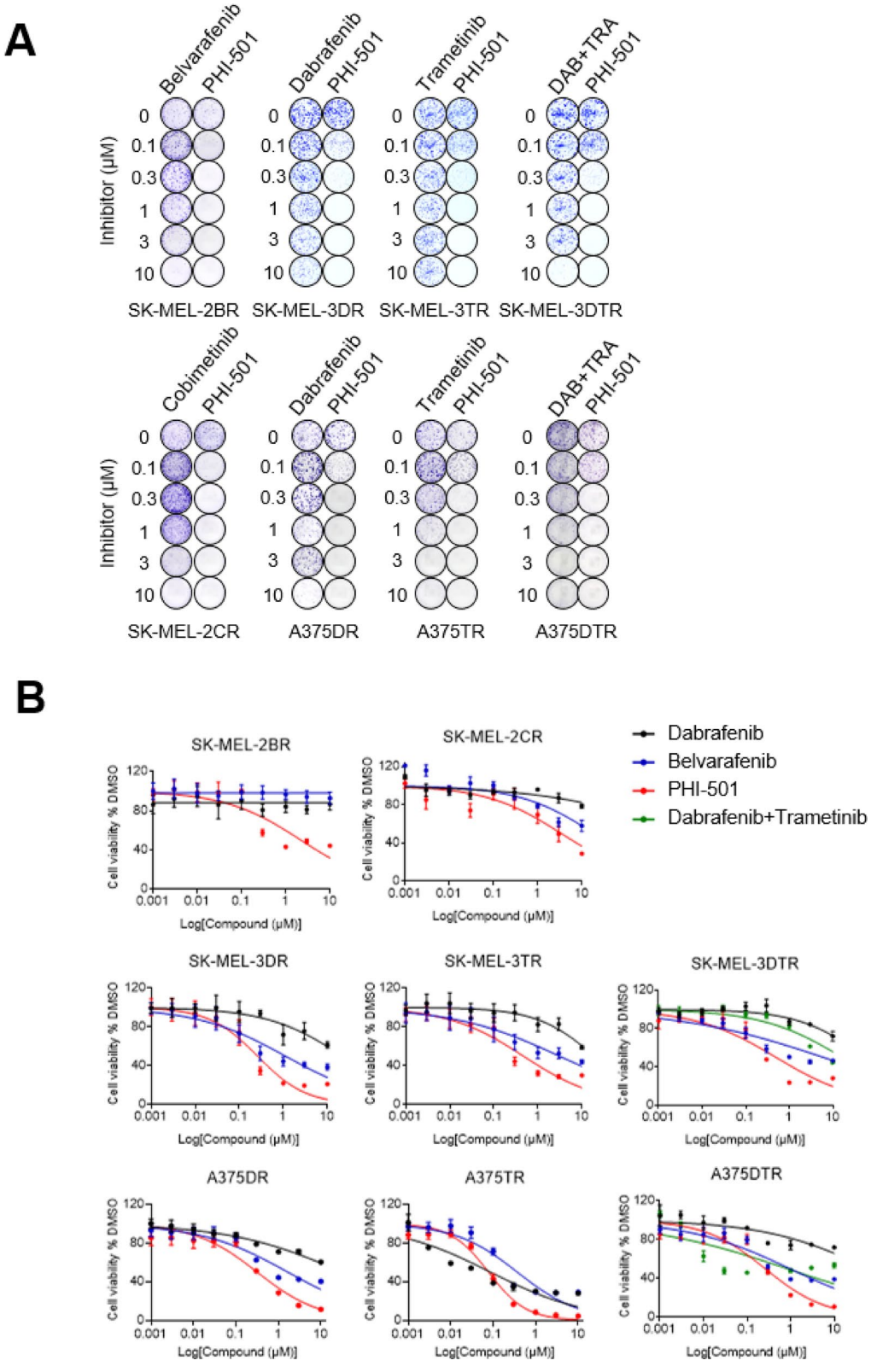

Fig. 5 (See legend on next page.)

(See figure on previous page.)

Fig. 5 PHI-501 Effectively Inhibits Growth and Suppresses MAPK and DDR Signaling in Drug-Resistant Melanoma Cells. (**A**) Clonogenic assay comparing the inhibitory effects of PHI-501 against belvarafenib, dabrafenib, trametinib, and the combination of dabrafenib plus trametinib (DAB + TRA) in drug-resistant melanoma cells. (**B**) Dose–response curves and GI_{50} values of belvarafenib, dabrafenib, dabrafenib + trametinib, and PHI-501 in resistant melanoma cells. Cells were treated with inhibitors (0.001–10 μM) or DMSO (vehicle) for 48 h. Data are presented as mean ± SEM. (**C**) Table summarizing the GI_{50} values shown in Fig. 5B. (**D**) Immunoblot analysis of pDDR1/2, pERK, pAKT and β-actin in resistant melanoma cell lines (SK-MEL-2BR, SK-MEL-2CR, SK-MEL-3DR, SK-MEL-3TR, and SK-MEL-3DTR) following 48-h treatment with the indicated inhibitors (1 or 10 μM). (**E**) Principal component analysis (PCA) of RNA-seq data from six melanoma cell lines (SK-MEL-2, SK-MEL-3, SK-MEL-2BR, SK-MEL-3DR, SK-MEL-3TR, and SK-MEL-3DTR) treated with 10 μM PHI-501 for 48 h. (**F**) Hierarchical clustering heatmap displaying the top 1000 most variable genes across all five cell lines treated with or without PHI-501. (**G**) GSEA enrichment plots for the MAPK signaling pathway in drug-resistant cells following PHI-501 treatment

SK-MEL-2 (parental and BR) group and the SK-MEL-3 (parental, DR, TR, and DTR) group. In both groups, samples were separated along PC1 according to control and PHI-501–treated conditions, with PC1 explaining 35.19% of the total variance in the SK-MEL-2 group and 40.9% in the SK-MEL-3 group. Biological replicates clustered consistently within each condition (Fig. 5e). Consistently, volcano plots of differential gene expression in resistant models further demonstrated broad transcriptional reprogramming following PHI-501 treatment (Supplementary Figure S6a).

Hierarchical clustering of the 1000 most variable genes further demonstrated that PHI-501 induced marked transcriptional changes in both parental and resistant melanoma cells (Fig. 5f). Kyoto Encyclopedia of Genes and Genomes (KEGG) and Hallmark GSEA performed in both parental and RAF-resistant melanoma cells following PHI-501 treatment consistently revealed pathway suppression. KEGG analysis showed significant downregulation of the MAPK signaling pathway gene set, and Hallmark analysis similarly demonstrated marked decreases in PI3K/AKT/mTOR signaling, KRAS signaling UP, and epithelial–mesenchymal transition gene sets (Supplementary Figure S6b and S6c). Notably, GSEA enrichment plots for MAPK signaling, PI3K/AKT/mTOR signaling, KRAS signaling UP, and epithelial–mesenchymal transition highlighted significant pathway suppression, with PHI-501 demonstrating inhibitory effects in resistant cells as well as in parental cells (Fig. 5g and Supplementary Figure S6d-S6f).

PHI-501 demonstrates in vivo antitumor efficacy in dabrafenib/trametinib–resistant melanoma models

The pharmacokinetic properties of PHI-501 were evaluated in BALB/c nude mice following a single intravenous (1 mg/kg) or oral (10 mg/kg) administration. After oral administration, PHI-501 exhibited rapid absorption (T_{max} = 0.5 h), achieving a C_{max} of 3.68 μg/mL, with a terminal half-life of 2.4 h and a high absolute bioavailability (Fig. 6a and b).

To assess the in vivo efficacy of PHI-501 in overcoming acquired resistance, we established two xenograft models: the dabrafenib-resistant SK-MEL-3DR and the dabrafenib/trametinib combination-resistant SK-MEL-3DTR. In the SK-MEL-3DR model, PHI-501 (30 mg/kg, b.i.d.) treatment resulted in a remarkable tumor growth inhibition (TGI) rate of 72.12%, significantly outperforming both the vehicle and dabrafenib (100 mg/kg, q.d.) groups (Fig. 6c). While the dabrafenib-treated group showed a TGI of − 7.42%, confirming the robustness of this resistance model, PHI-501 led to significant reductions in both tumor weight and volume (Fig. 6c and e). Consistent with these observations, immunoblotting of excised SK-MEL-3DR tumors revealed that PHI-501 significantly suppressed the phosphorylation of DDR1/2, MEK1/2, and ERK1/2, whereas changes in AKT phosphorylation were not statistically significant (Fig. 6f and g). To further evaluate PHI-501 in a more clinically challenging context, we performed xenograft studies using the SK-MEL-3DTR model, which mimics resistance to BRAF/MEK combination therapy. In this model, PHI-501 demonstrated the most potent anti-tumor activity and was the only treatment that achieved a statistically significant reduction in tumor growth compared to the vehicle control ($p = 0.0012$) (Fig. 6h, Supplementary Figure S7d). No significant body weight loss was observed in either model during PHI-501 treatment (Supplementary Fig. S7a–c). These findings highlight PHI-501 as a promising therapeutic strategy to

C

Cell line	GI50 (μM)		
	PHI-501	Dabrafenib	Belvarafenib
SK-MEL-2BR	2.2160	NA	NA
SK-MEL-2CR	3.4240	NA	18.960
SK-MEL-3DR	0.2602	22.44	1.120
SK-MEL-3TR	0.4694	19.38	3.079
SK-MEL-3DTR	0.4974	54.93	6.094
A375DR	0.3172	32.15	1.675
A375TR	0.07795	0.08714	0.3712
A375DTR	0.2622	63.50	0.9733

D

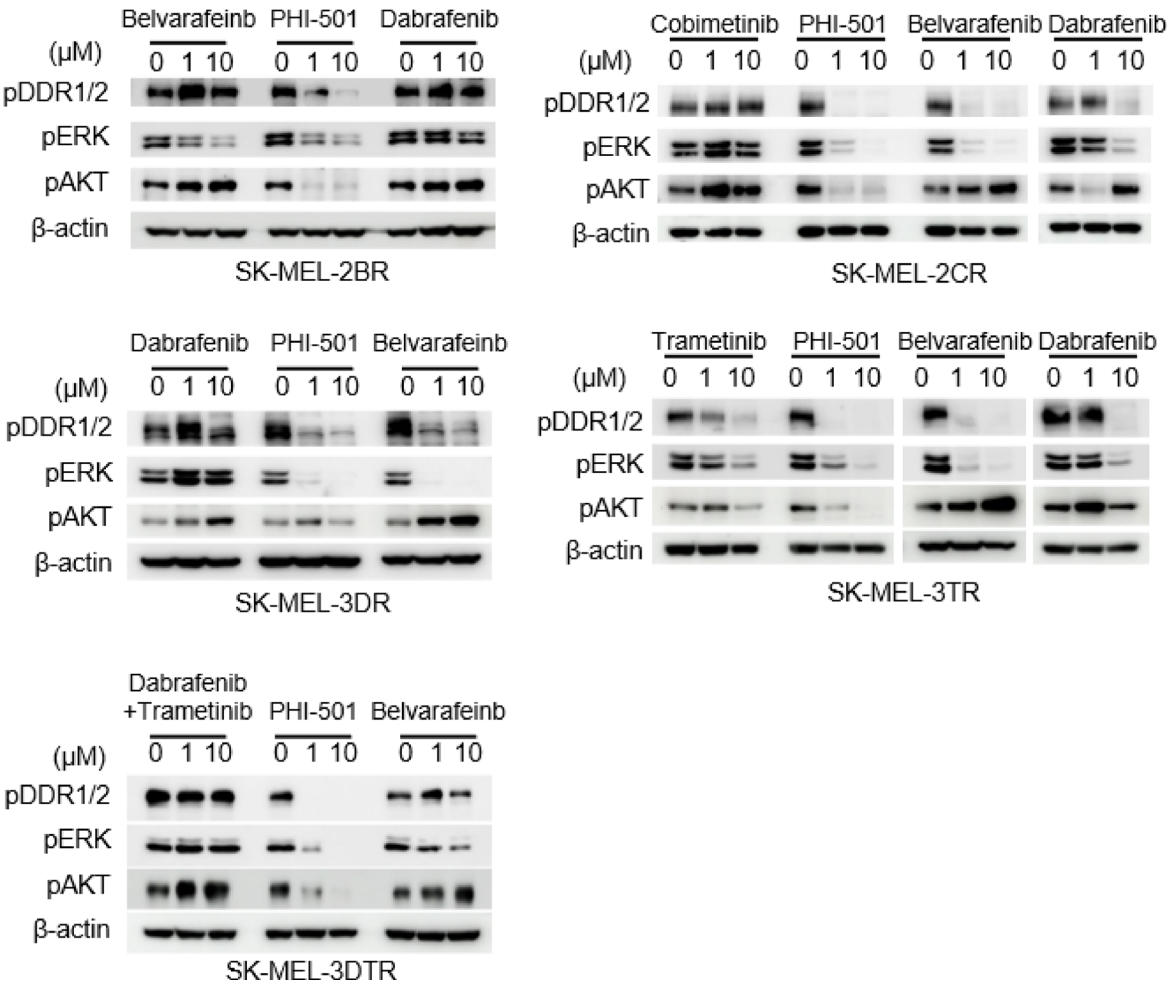

Fig. 5 (continued)

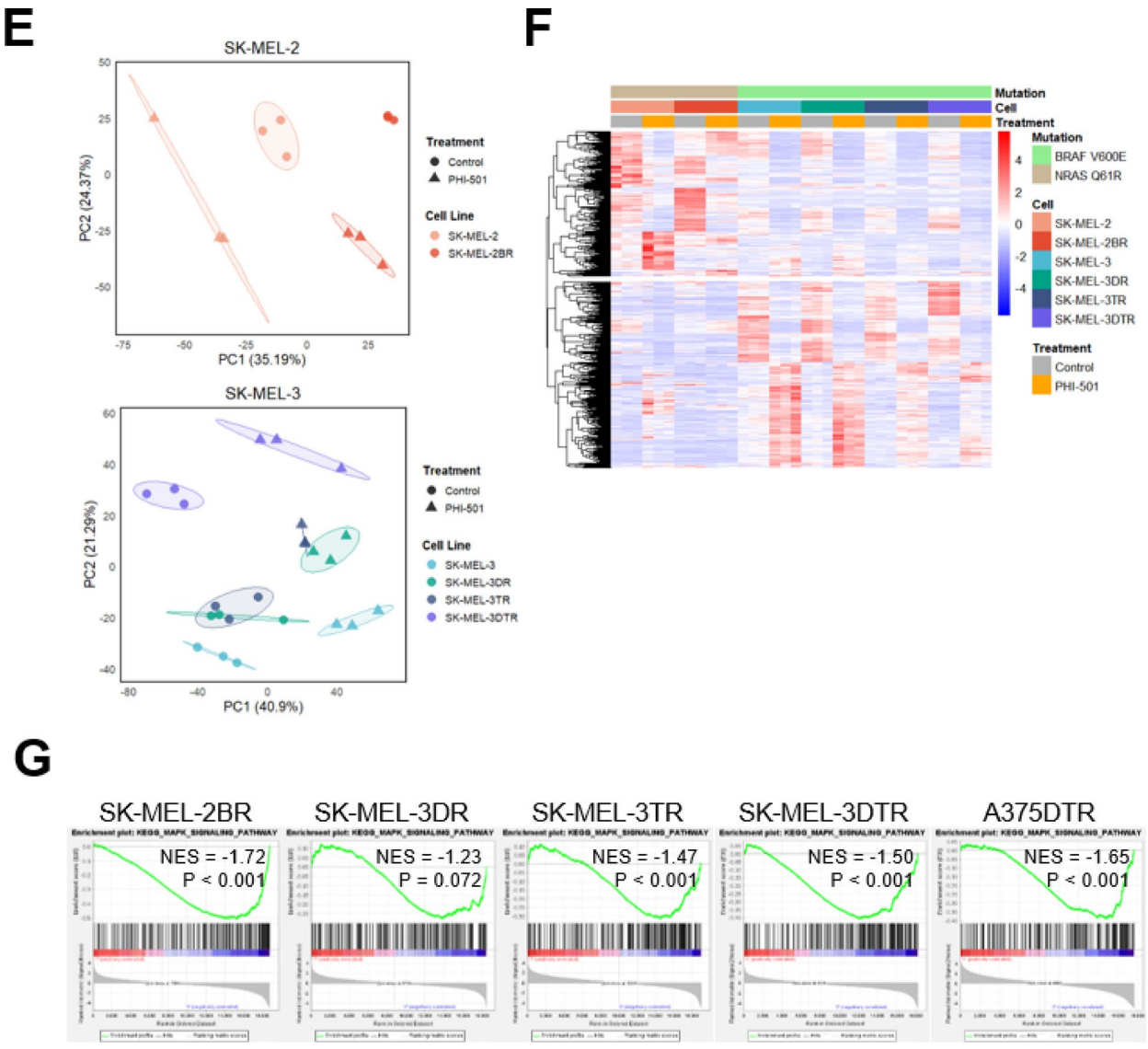

Fig. 5 (continued)

overcome dabrafenib and trametinib resistance in melanoma by targeting the critical signaling pathways involved in tumor survival and progression.

Discussion

Targeted therapies, including BRAF and MEK inhibitors and immune checkpoint blockade, have significantly improved the survival rates of patients with advanced melanoma [29, 30]. For BRAF V600-mutant melanoma (40–50% of cases), combination therapy offers enhanced initial response rates and survival benefits [31]. However, these responses are typically transient, with most patients developing resistance within 12–15 months through MAPK pathway reactivation (via secondary RAS mutations, BRAF splice variants, or amplification), compensatory PI3K–AKT signaling, alternative RTK upregulation, and tumor microenvironment remodeling [32, 33]. NRAS-mutant melanoma (15–20% of cases) presents a significant therapeutic challenge. MEK inhibitors provide only modest benefits, whereas RAF inhibitors are clinically ineffective owing to the wild-type RAF paradox [34]. Consequently, most NRAS-mutant

A

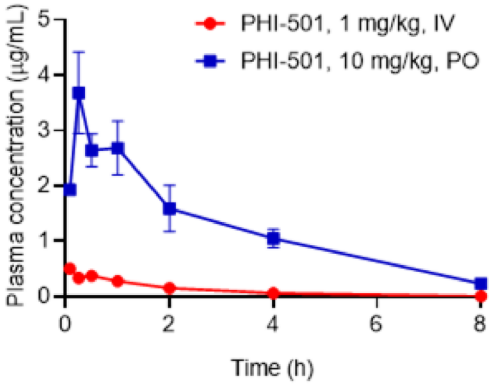

B

Route	i.v.	p.o.
Dose (mg/kg)	1	10
C0 (ng/mL)	613.78	
Cmax (ng/mL)		3677.00
Tmax (hr)		0.50
AUCinf (ng·hr/mL)	951.05	15254.87
t1/2 (hr)	1.40	2.4
CL (mL/hr/kg)	1051.47	
Vdss (mL/kg)	2120.26	
Bioavailability (%)		160.4

C

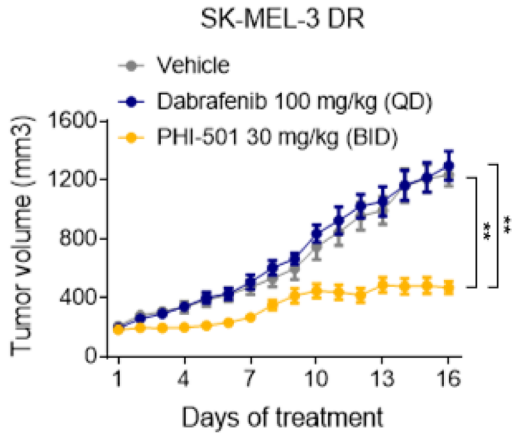

D

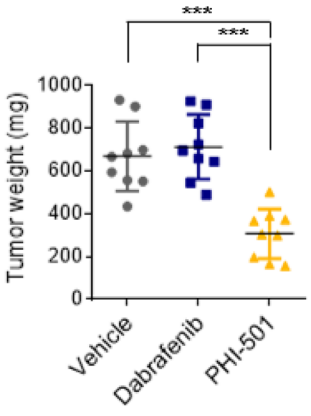

E

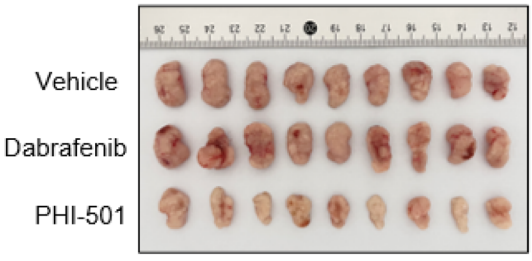

F

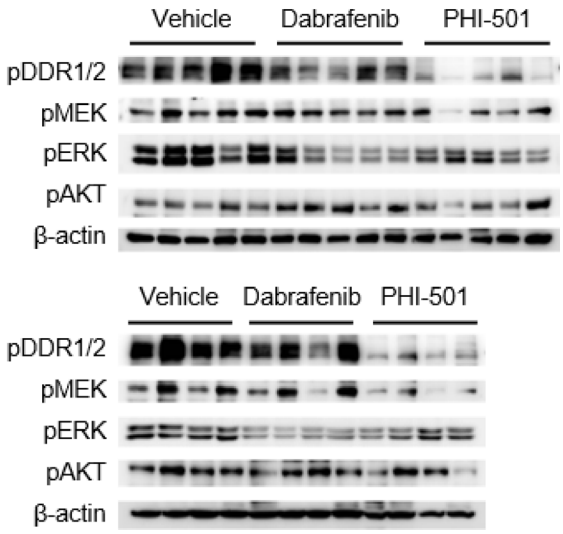

Fig. 6 (See legend on next page.)

(See figure on previous page.)

Fig. 6 PHI-501 demonstrates in vivo antitumor efficacy in dabrafenib/trametinib–resistant melanoma models. (**A**) Plasma concentration–time profiles of PHI-501 (i.v. at 1 mg/kg and p.o. at 5, 10, or 30 mg/kg, $n = 3$). (**B**) Pharmacokinetic parameters for PHI-501 after i.v. (1 mg/kg) and p.o. (10 mg/kg) dosing, including C_0, C_{max}, T_{max}, AUC_{inf}, elimination half-life ($t_{1/2}$), clearance (CL), volume of distribution (Vdss), and oral bioavailability. (**C**) SK-MEL-3DR xenograft in BALB/c nude mice. Vehicle or PHI-501 was orally administered as indicated ($n = 9$). Data are presented as the mean ± SEM. (**D**) Tumor weights at the endpoint of the study for the SK-MEL-3DR xenograft model. Data are presented as the mean ± SD. (**E**) Representative tumor images from SK-MEL-3DR xenograft in each treatment group at the study endpoint. (**F**) Western blot analysis of tumors from SK-MEL-3DR xenograft pDDR1/2, pMEK, pERK, pAKT, and β-actin. (**G**) Quantification of pDDR1/2, pMEK, pERK, and pAKT normalized to β-actin from the western blot analysis shown in (F). Data are presented as mean ± SEM ($n = 9$). (**H**) SK-MEL-3DTR xenograft in BALB/c nude mice. Vehicle, dabrafenib+trametinib, belvarafenib or PHI-501 was orally administered as indicated ($n = 5$). Data are presented as the mean ± SEM

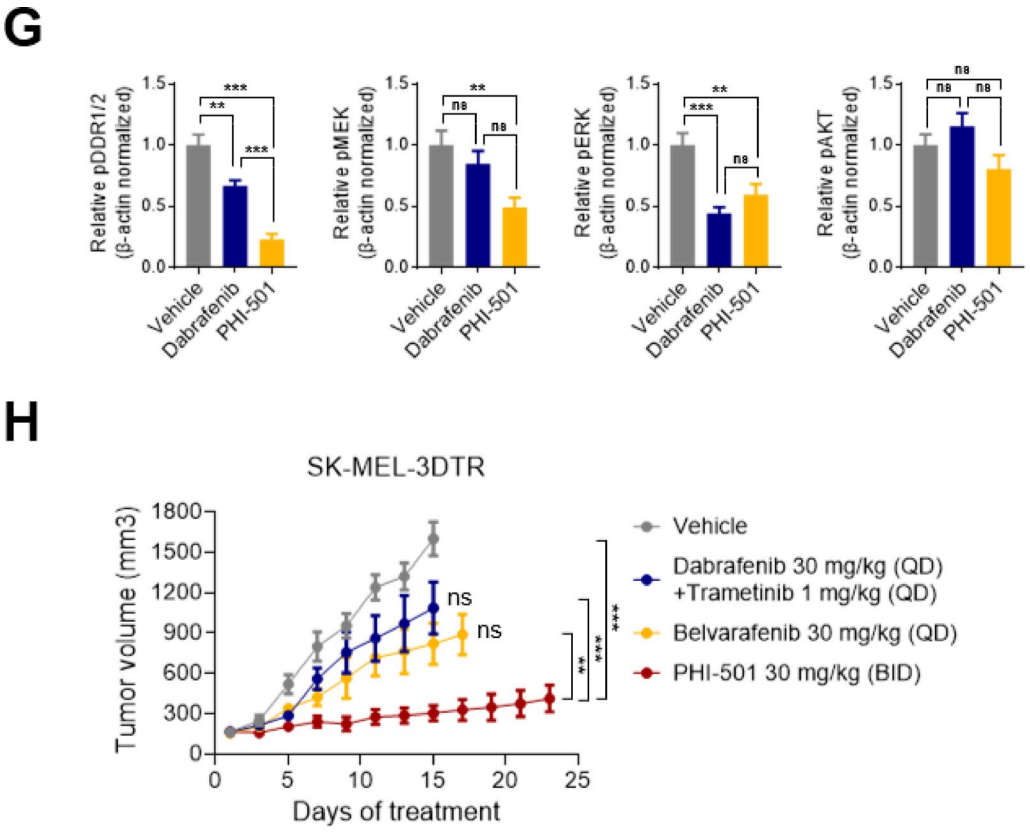

Fig. 6 (continued)

patients rely on immunotherapy, leaving limited options for those who are unresponsive to immune checkpoint inhibition [35].

Recent therapeutic strategies have focused on the comprehensive MAPK pathway targeting and resistance mechanisms [36, 37]. "Paradox breaker" pan-RAF inhibitors (e.g., naporafenib) and ERK inhibitors show promise in early trials, particularly for NRAS-mutant disease [38]. However, resistance often re-emerges through adaptive mechanisms, such as ARAF mutations or microenvironment-driven escape [39]. Current approaches have inadequately addressed tumor plasticity and the contribution of collagen-dense microenvironments to treatment resistance.

This landscape highlights the urgent need for innovative therapies that concurrently target both canonical signaling and adaptive resistance mechanisms in melanoma. Our study introduced PHI-501, a dual pan-RAF/DDR1/2 inhibitor, as a novel approach to address these challenges in BRAF- and NRAS-driven melanoma. PHI-501 demonstrated superior efficacy in overcoming resistance compared to existing agents, required lower doses, and exhibited favorable pharmacokinetics and toxicity profiles.

These findings provide preclinical evidence that PHI-501 attenuates MAPK- and DDR-associated signaling and exhibits anti-tumor activity in experimental models of MAPK inhibitor–resistant melanoma. Potential translational considerations, including biomarkers related to DDR1/2 expression, ECM-associated transcriptional programs, or MAPK pathway activation, remain as hypotheses requiring further validation. Likewise, any potential

implications for immune exclusion or combination strategies with immune checkpoint blockade remain to be empirically determined, as these were not evaluated in immunocompetent models. Such possibilities warrant dedicated future studies to fully assess complex tumor–immune and tumor–stroma interactions.

PHI-501 has recently been cleared by the Korean Ministry of Food and Drug Safety (MFDS) for a Phase 1 clinical trial, which will allow for the initial evaluation of its safety and biological activity in humans. While the current study focused on melanoma, the dual inhibition of pan-RAF and DDR1/2 might also be relevant in other oncology contexts where MAPK activation and collagen-rich stroma contribute to resistance. Future research would be required to empirically determine whether these preclinical findings can be extended to other malignancy types and to identify relevant predictive biomarkers.

Limitations of the study

Despite these findings, our study has several limitations. First, while increased DDR1/2 expression and signaling changes were consistently observed in resistant models, the present study does not include functional gain- or loss-of-function experiments to establish a causal role for DDR1 or DDR2 in driving resistance. Second, our in vivo efficacy data were generated in xenograft models derived from BRAF V600E (class 1) melanoma, and we did not evaluate PHI-501 in NRAS-mutant xenograft models or in melanoma models harboring class 2/3 BRAF alterations. Third, because the xenograft studies were performed in immunodeficient mice, we could not assess tumor–immune interactions or test combinations with immune checkpoint blockade. Future studies incorporating NRAS-mutant xenografts, patient-derived xenografts, 3D organoids, and genetically engineered mouse models will be important to evaluate PHI-501 in more physiologically relevant preclinical contexts and to define determinants of response and potential resistance mechanisms.

Conclusion

PHI-501 is a dual inhibitor targeting pan-RAF and DDR1/2 kinases and, in our experimental models, suppressed MAPK- and DDR-associated signaling. Across BRAF- and NRAS-mutant melanoma cell models with acquired resistance to MAPK pathway inhibitors, PHI-501 showed anti-tumor activity in vitro and in xenograft studies, together with a pharmacokinetic profile and tolerability in mice consistent with further investigation. Collectively, these results support further preclinical evaluation of PHI-501 in models of resistance to current MAPK-targeted therapies and help inform the design of future translational studies.

Abbreviations

DDR / DDR1/2	Discoidin domain receptor 1/2
MAPK	Mitogen-activated protein kinase
MEK	Mitogen-activated protein kinase kinase
ERK	Extracellular signal-regulated kinase
AKT	Protein kinase B
PI3K	Phosphoinositide 3-kinase
mTOR	Mammalian target of rapamycin
ECM	Extracellular matrix
EMT	Epithelial-mesenchymal transition
GSEA	Gene Set Enrichment Analysis
WES	Whole-exome sequencing
SNV	Single-nucleotide variant
CNV	Copy number variation
RPPA	Reverse phase protein array
PDX	Patient-derived xenograft
CCK-8	Cell Counting Kit-8 assay
RPPA	Reverse Phase Protein Array
TCGA-SKCM	The Cancer Genome Atlas, Skin Cutaneous Melanoma dataset
CCLE	Cancer Cell Line Encyclopedia
DepMap	Dependency Map database
GDSC / GDSC2	Genomics of Drug Sensitivity in Cancer database
NES	Normalized Enrichment Score
FDR	False Discovery Rate
GEPIA2	Gene Expression Profiling Interactive Analysis 2 web tool
TGI	Tumor Growth Inhibition
QD	Quaque die (Once a day)
BID	Bis in die (Twice a day)

Supplementary Information

The online version contains supplementary material available at https://doi.org/10.1186/s12935-026-04271-w.

Supplementary Material 1.

Supplementary Material 2.

Supplementary Material 3.

Supplementary Material 4.

Acknowledgements

Not applicable.

Author contributions

SMK conceptualized the study, designed the methodology, contributed to the establishment of cell lines, performed cell and animal experiments, carried out RNA sequencing analysis, and wrote the original draft.SC participated in the animal experiments, contributed to data curation, and was involved in drafting the manuscript.GJS validated the results through CCK-8 assay and contributed to drafting the manuscript.KYN provided the kinase assay data, provided resources, and contributed to the review and editing of the manuscript.JHY participated in the design of the study and provided resources.TS contributed to revising the manuscript and assisted with reviewing and editing.JBA contributed to revising the manuscript and assisted with reviewing and editing.SJS conceptualized the study, supervised the project, managed project administration, and contributed to writing – review & editing.All authors read and approved the final manuscript.

Funding

This research was supported by Pharos iBio Co., Ltd.

Data availability

The RNA-seq data generated during this study are available from the corresponding author upon reasonable request. All other data supporting the findings of this study are available from the corresponding author upon reasonable request. No custom code was generated or used in this study.

Declarations

Consent for publication
Not applicable.

Competing interests
K-Y. N. & J.H.Y. are employers and current equity holder at Pharos iBio Co., Ltd. G-J.S. is an employee at Pharos iBio Co., Ltd.

Author details
[1]Department of Medicine, Yonsei University College of Medicine, Seoul 03722, Republic of Korea
[2]Songdang Institute for Cancer Research, Yonsei University College of Medicine, Seoul 03722, Republic of Korea
[3]Pharos iBio Co., Ltd, Anyang-si, South Korea
[4]Department of Medical Science, Graduate School of Medical Science, Brain Korea 21 Project, Yonsei University College of Medicine, Seoul 03722, Republic of Korea
[5]Department of Biomedical Sciences, Yonsei University College of Medicine, Seoul 03722, Republic of Korea
[6]Graduate School of Clinical Drug Discovery & Development, Yonsei University College of Medicine, Seoul 03722, Republic of Korea
[7]Clinical Candidate Discovery & Development Institute, Yonsei University College of Medicine, Seoul 03722, Republic of Korea
[8]Division of Medical Oncology, Department of Internal Medicine, Yonsei Cancer Center, Yonsei University College of Medicine, Seoul, Republic of Korea

Received: 30 September 2025 / Accepted: 12 March 2026
Published online: 04 April 2026

References
1. Davis EJ, Johnson DB, Sosman JA, Chandra S. Melanoma: what do all the mutations mean. Cancer. 2018;124:3490–9. https://doi.org/10.1002/cncr.31345.
2. Randic T, Kozar I, Margue C, Utikal J, Kreis S. NRAS mutant melanoma: towards better therapies. Cancer Treat Rev. 2021;99:102238. https://doi.org/10.1016/j.ctrv.2021.102238.
3. Imani S, Roozitalab G, Emadi M, Moradi A, Behzadi P, Jabbarzadeh Kaboli P. The evolution of BRAF-targeted therapies in melanoma: overcoming hurdles and unleashing novel strategies. Front Oncol. 2024;14:1504142. https://doi.org/10.3389/fonc.2024.1504142.
4. Subbiah V, Baik C, Kirkwood JM. Clinical development of BRAF plus MEK inhibitor combinations. Trends Cancer. 2020;6:797–810. https://doi.org/10.1016/j.trecan.2020.05.009.
5. Luke JJ, Flaherty KT, Ribas A, Long GV, Grob JJ. Targeted agents and immunotherapies: prime time for re-evaluation in melanoma? Nat Rev Clin Oncol. 2022;19(11):741–58. https://doi.org/10.1038/s41571-022-00679-6.
6. Robert C, Karaszewska B, Schachter J, Rutkowski P, Mackiewicz A, Stroiakovski D, et al. Improved overall survival in melanoma with combined dabrafenib and trametinib. N Engl J Med. 2015;372(1):30–9. https://doi.org/10.1056/NEJMoa1412690.
7. Dummer R, Ascierto PA, Gutzmer R, Drilon A, Rutkowski P, Kirkwood JM, et al. Encorafenib plus binimetinib versus vemurafenib or encorafenib in patients with BRAF-mutant melanoma (COLUMBUS): a multicentre, open-label, randomised phase 3 trial. Lancet Oncol. 2018;19(9):1151–63. https://doi.org/10.1016/S1470-2045(18)30376-1.
8. Ascierto PA, McArthur GA, Dréno B, Atkinson V, Liszkay G, Di Giacomo AM, et al. Cobimetinib combined with vemurafenib in advanced BRAFV600-mutant melanoma (coBRIM): updated efficacy results from a randomised, double-blind, phase 3 trial. Lancet Oncol. 2016;17(9):1248–60. https://doi.org/10.1016/S1470-2045(16)30122-X.
9. Hugo W, Shi H, Sun L, Piva M, Song C, Conglianese DN, et al. Non-genomic amplification of MEK and RAF confers resistance to the targeted RAF inhibitor vemurafenib in melanoma. Cell. 2015;162(3):564–74. https://doi.org/10.1016/j.cell.2015.06.046.
10. Adelmann CH, Ching G, Du L, Saporito RC, Bansal V, Pence LJ, et al. Comparative profiles of BRAF inhibitors: the paradox index as a predictor of clinical toxicity. Oncotarget. 2016;7:30453–60. https://doi.org/10.18632/oncotarget.8351.
11. Holderfield M, Nagel TE, Stuart DD. Mechanism and consequences of RAF kinase activation by small-molecule inhibitors. Br J Cancer. 2014;111:640–5. https://doi.org/10.1038/bjc.2014.139.
12. Kilburn LB, Liu D, Dorris K, et al. The type II RAF inhibitor tovorafenib in relapsed/refractory pediatric low-grade glioma: the phase 2 FIREFLY-1 study. Nat Med. 2023;29(12):3179–89. https://doi.org/10.1038/s41591-023-02668-y.
13. Tkacik ET, Parikh K, Li J, et al. Structure and RAF family kinase isoform selectivity of type II RAF inhibitors. J Biol Chem. 2023;299(8):104933. https://doi.org/10.1016/j.jbc.2023.104933.
14. Sun JM, Lim SM, Lee SH, et al. A phase Ib trial of belvarafenib in combination with cobimetinib in patients with NRAS-mutant melanoma: dose-expansion results. J Clin Oncol. 2021;39(15suppl):3007. https://doi.org/10.1200/JCO.2021.39.15_suppl.3007.
15. FDA Oncology Center of Excellence. Tovorafenib for relapsed or refractory BRAF-altered pediatric low-grade glioma. Oncologist. 2025;30(5):e1–10. https://doi.org/10.1093/oncolo/opae085.
16. Kline CN, Kilburn LB, Liu D, et al. Preclinical activity of the type II RAF inhibitor tovorafenib in BRAF-altered pediatric low-grade glioma models. Neuro Oncol. 2025;27(5):1341–50. https://doi.org/10.1093/neuonc/noae123.
17. Rammal H, Saby C, Magnien K, et al. Discoidin domain receptors: microenvironment sensors that promote cellular migration and invasion. Cell Adh Migr. 2016;10(4):368–77. https://doi.org/10.1080/19336918.2016.1178447.
18. Béraud C, Montbarbon E, Berthelot L, et al. Discoidin domain receptors orchestrate cancer progression: a focus on melanoma. Cancer Sci. 2021;112(5):1722–33. https://doi.org/10.1111/cas.14789.
19. Aguilera A, Castillo-Sánchez L, Hernández-Fernández JL, et al. Discoidin domain receptors in melanoma: potential therapeutic targets. Front Oncol. 2020;10:1748. https://doi.org/10.3389/fonc.2020.01748.
20. Berestjuk I, et al. Targeting discoidin domain receptors DDR1 and DDR2 overcomes matrix-mediated tumor cell adaptation and tolerance to BRAF-targeted therapy in melanoma. EMBO Mol Med. 2022;14(2):e14905. https://doi.org/10.15252/emmm.202114905.
21. Aguilera A, et al. Discoidin domain receptor 2 promotes melanoma metastasis and is a therapeutically accessible target. Pigment Cell Melanoma Res. 2021;34(4):678–90. https://doi.org/10.1111/pcmr.12958.
22. Kolb A, Maat W, Jansen S, et al. A phase II trial of dasatinib in advanced melanoma. Invest New Drugs. 2011;29(6):1406–11. https://doi.org/10.1007/s10637-010-9523-6.
23. Wu J, et al. Dasatinib inhibits primary melanoma cell proliferation and migration and overcomes resistance to MAPK pathway inhibition. Oncol Rep. 2013;29(2):585–92. https://doi.org/10.3892/or.2012.2133.
24. Song J, Chen X, Bai J, Liu Q, Li H, Xie J, et al. Discoidin domain receptor 1 (DDR1), a promising biomarker, induces epithelial to mesenchymal transition in renal cancer cells. Tumour Biol. 2016;37:11509–21. https://doi.org/10.1007/s13277-016-5021-2.
25. Walsh LA, Nawshad A, Medici D. Discoidin domain receptor 2 is a critical regulator of epithelial-mesenchymal transition. Matrix Biol. 2011;30:243–7. https://doi.org/10.1016/j.matbio.2011.03.007.
26. Sala M, Allain N, Moreau M, Jabouille A, Henriet E, Abou-Hammoud A, et al. Discoidin domain receptor 2 orchestrates melanoma resistance combining phenotype switching and proliferation. Oncogene. 2022;41:2571–86. https://doi.org/10.1038/s41388-022-02266-1.
27. Ruiz PA, Jarai G. Collagen I induces discoidin domain receptor 1 expression through discoidin domain receptor 2 and a JAK2-ERK1/2-mediated mechanism in primary human lung fibroblasts. J Biol Chem. 2011;286:12912–23. https://doi.org/10.1074/jbc.M110.143693.
28. Yeh YC, Lin HH, Tang MJ. Dichotomy of the function of DDR1 in cells and disease progression. Biochim Biophys Acta Mol Cell Res. 2019;1866:118473. https://doi.org/10.1016/j.bbamcr.2019.04.003.
29. Wang Y, Almanzar R, Williams A, et al. Clinical predictors of survival in patients with BRAF V600-mutated metastatic melanoma treated with first-line immune checkpoint inhibitors or BRAF/MEK inhibitors. Oncologist. 2024;29:e507–14. https://doi.org/10.1093/oncolo/oyae054.
30. Boutros C, Mihalcioiu C, Hao D. The treatment of advanced melanoma: current approaches and future directions. Crit Rev Oncol Hematol. 2020;153:103013.
31. Long GV, Stroyakovskiy D, Gogas H, Levchenko E, de Braud F, Larkin J, et al. Combined BRAF and MEK inhibition versus BRAF inhibition alone in melanoma. N Engl J Med. 2014;371:1877–88. https://doi.org/10.1056/NEJMoa1406037.
32. Sun C, Wang L, Huang S, Heynen GJ, Prahallad A, Robert C, et al. Reversible and adaptive resistance to BRAF(V600E) inhibition in melanoma. Nature. 2014;508:118–22. https://doi.org/10.1038/nature13121.

33. Villanueva J, Vultur A, Herlyn M. Acquired resistance to BRAF inhibitors mediated by a RAF kinase switch in melanoma can be overcome by cotargeting MEK and IGF-1R/PI3K. Cancer Cell. 2010;18:683–95. https://doi.org/10.1016/j.ccr.2010.11.023.
34. Wei X, Lu S, Li P, Ma X, Zhou J, Wei S, et al. A phase II study of efficacy and safety of the MEK inhibitor tunlametinib in patients with unresectable NRAS-mutant melanoma. J Clin Oncol. 2024;42:e21545. https://doi.org/10.1200/JCO.2024.42.16_suppl.e21545.
35. Larkin J, Chiarion-Sileni V, Gonzalez R, Grob JJ, Cowey CL, Lao CD, et al. Combined nivolumab and ipilimumab or monotherapy in untreated melanoma. N Engl J Med. 2015;373:23–34. https://doi.org/10.1056/NEJMoa1504030.
36. Yao Z, Yaeger R, Rodrik-Outmezguine VS, Tao A, Fernandez M, Chang MT, et al. Tumours with class 3 BRAF mutants are sensitive to the inhibition of activated RAS. Nature. 2017;548:234–8. https://doi.org/10.1038/nature23291.
37. Sullivan RJ, Flaherty KT, Infante JR, Rodon J, Bendell JC, Ramelyte E, et al. A phase I study of LXH254, a type II pan-RAF inhibitor, in patients with advanced solid tumors. J Clin Oncol. 2022;40:9514. https://doi.org/10.1200/JCO.2022.40.16_suppl.9514.
38. Lehr HA, Heinzerling L, Keilholz U, Reinmuth S, et al. Naporafenib plus trametinib in patients with NRAS-mutant or BRAF-mutant melanoma: a phase Ib/II trial. Nat Med. 2022;28:2634–43. https://doi.org/10.1038/s41591-022-02050-0.
39. Van Allen EM, Wagle N, Sucker A, Treacy DJ, Johannessen CM, Goetz EM, et al. The genetic landscape of clinical resistance to RAF inhibition in metastatic melanoma. Cancer Discov. 2014;4:94–109. https://doi.org/10.1158/2159-8290.CD-13-0633.

Publisher's note